Alkyne-Protected Ruthenium Nanoparticles[†]

Wei Chen,[‡] Nathaniel B. Zuckerman, Xiongwu Kang, Debraj Ghosh, Joseph P. Konopelski, and Shaowei Chen*

Department of Chemistry and Biochemistry, University of California, 1156 High Street, Santa Cruz, California 95064

Received: February 3, 2010; Revised Manuscript Received: March 9, 2010

Stable ruthenium nanoparticles protected by 1-octynyl fragments were synthesized by a wet chemical method. Transmission electron microscopic measurements showed that the resulting particles exhibited an average core diameter of 2.55 ± 0.15 nm with well-defined Ru crystalline lattice fringes. Because of the formation of Ru—C≡ bonds, the C≡C vibrational stretch was found in FTIR measurements to red-shift to 1936 cm^{-1} from 2119 cm^{-1} that was observed for monomeric 1-octyne. Interestingly, the nanoparticles underwent ligand exchange reactions with alkynyl lithium (e.g., 5-phenyl-1-pentynyl lithium) for further surface functionalization, as manifested in FTIR as well as ^{1}H and ^{13}C NMR measurements. Optically, whereas UV−vis absorption measurements exhibited only a featureless profile, the Ru nanoparticles displayed apparent photoluminescence with an emission peak at 428 nm, which was accounted for by intraparticle charge delocalization as a consequence of the strong Ru—C≡ bonds and the conducting Ru metal cores such that the particle bound C≡C moieties behaved analogously to diacetylene derivatives. The impacts of the interfacial bonding interactions on intraparticle charge delocalization were further illustrated by Ru nanoparticles functionalized with a mixed monolayer of both octyne and ethynylferrocene ligands. At a ferrocene surface coverage of ca. 13%, electrochemical measurements depicted two pairs of voltammetric peaks with a potential spacing of 265 mV. A new NIR absorption band centered around 1687 nm also started to emerge with the addition of nitrosonium tetrafluoroborate ($NOBF_4$) as the oxidizing reagent and the peak intensity exhibited a volcano-shape dependence on the amount of $NOBF_4$ added. These observations strongly suggested that there existed effective intervalence charge transfer between the particle-bound ferrocene groups at mixed valence, analogous to the observation where the ferrocene moieties were bound onto the particle surface by Ru—carbene π bonds.

Introduction

The research interests in nanoparticle materials have been primarily motivated by the unique chemical and physical properties that may be enormously different from those of the corresponding bulk materials or constituent atoms,[1–3] and their diverse potential applications in nanoelectronics,[4–7] (electro)catalysis,[8–12] chemical/biological sensing,[13–19] data storage,[20,21] etc. Of these, monolayer-protected metal nanoparticles represent a unique class of nanomaterials that may be exploited as nanoscale building blocks for the construction of advanced functional nanostructures.[22] Because of the nanocomposite nature, the particle material properties can be readily manipulated not only by the metal cores but also by the organic protecting layers as well as the metal−ligand interfacial bonding interactions.[23,24]

Whereas mercapto derivatives have been used extensively as the ligands of choice for nanoparticle surface passivation because of the strong affinity of thiol groups to transition metal surfaces,[18,25,26] recently several studies have shown that transition-metal nanoparticles, such as Au, Pt, Ti, Ru, and Pd, may also be passivated by stable metal—carbon covalent bonds.[4,27–30] Notably, the optoelectronic properties of the resulting particle materials were found to deviate rather significantly from those of the mercapto-stabilized counterparts. For instance, ruthenium nanoparticles stabilized by metal—carbene π bonds (Ru═C) have been found to exhibit apparent intraparticle charge delocalization, leading to the formation of an extended conjugation system between the particle-bound functional moieties.[4] This has recently been exemplified by the intervalence charge transfer between ferrocenyl moieties bound to ruthenium nanoparticles and the novel fluorescence characteristics of pyrene-functionalized ruthenium nanoparticles.[4,28,31] In addition, using diazonium derivatives as the precursors, various metal nanoparticles (e.g., Pd, Ti, and Ru) were also prepared by virtue of the formation of metal—carbon single bonds. In comparison to the alkanethiolate-passivated counterparts, these nanoparticles exhibited unusually high electronic conductivity, which was ascribed to the strong interfacial bonding interactions and low contact resistance that led to extended spilling of core electrons into the organic supporting matrix.[29,30,32]

In the present study, alkynes were used as a new type of protecting ligands for the stabilization of ruthenium nanoparticles by the formation of Ru—C≡ bonds. To the best of our knowledge, this is the first report of metal nanoparticles passivated by M—C≡ bonds. The resulting nanoparticles were then subject to detailed characterizations by a wide array of spectroscopic and microscopic measurements, including transmission electron microscopy (TEM), thermogravimetric analysis (TGA), Fourier-transformed infrared (FTIR), ultraviolet−visible (UV−vis) absorption, photoluminescence, ^{1}H and ^{13}C nuclear

[†] Originally intended for publication in the special issue "Protected Metallic Clusters, Quantum Wells and Metal-Nanocrystal Molecules Symposium", published as the September 30, 2010, issue of *J. Phys. Chem. C* (Vol. 114, issue 38; URL: http://pubs.acs.org/toc/jpccck/114/38).

* To whom correspondence should be addressed. E-mail: schen@chemistry.ucsc.edu.

[‡] Present address: State Key Laboratory of Electroanalytical Chemistry, Changchun Institute of Applied Chemistry, Chinese Academy of Sciences, Changchun 130022, China.

10.1021/jp101053c
Published on Web 03/25/2010

SCHEME 1

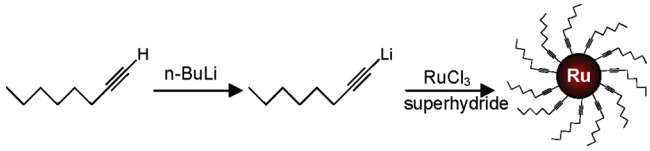

magnetic resonance (NMR) spectroscopy, as well as electrochemistry. Interestingly, the alkynyl-passivated nanoparticles also underwent ligand exchange reactions with lithium acetylide for further surface chemical functionalization. Furthermore, the impacts of the interfacial bonding interactions on nanoparticle charge transfer and optical properties, in particular, intraparticle charge delocalization, were examined in electrochemical and spectroscopic measurements by the incorporation of ferrocene moieties into the particle protecting monolayer.

Experimental Section

Chemicals. Ruthenium chloride ($RuCl_3$, 99+%, ACROS), superhydride ($LiB(C_2H_5)_3H$, 1 M in THF, ACROS), 1-octyne (Alfa Aesar, 98%), 5-phenyl-1-pentyne (Alfa Aesar, 98+%), triphenylphosphine (PPh_3, 99%, ACROS), and *n*-butyllithium (*n*-BuLi, ACROS) were used as received. All solvents were obtained from typical commercial sources and used without further treatment. Water was supplied by a Barnstead Nanopure water system (18.3 MΩ·cm).

Ethynylferrocene. 1,1-Dichloro-2-ferrocenylethene was first prepared according to Luo et al.[33] To a two-neck round-bottom flask under dry nitrogen was added PPh_3 (5.24 g, 20 mmol), ferrocenecarboxaldehyde (1.07 g, 5 mmol), and CH_3CN (10 mL, anhydrous). The solution was cooled to 0 °C, and CCl_4 was added in one portion. Stirring was continued at room temperature for 30 min, followed by addition of Nanopure water (5 mL). The mixture was then extracted with ether, washed with water, brine, and dried with $MgSO_4$. Following removal of solvent under reduced pressure, the residue was purified on a short column of neutral alumina (hexanes) (0.72 g, 51% yield). mp 56−57 °C (lit. 57−58 °C). ^{1}H NMR (600 MHz, $CDCl_3$) δ 6.53 (s, 1H), 4.58 (t, J = 1.8 Hz, 2H), 4.29 (t, J = 1.8 Hz, 2H), 4.18 (s, 5H). ^{13}C NMR (150 MHz, $CDCl_3$) δ 127.3, 116.2, 77.8, 69.3, 69.1. IR (cm^{-1}) 3368, 3111, 3025, 2917, 1786, 1725, 1622, 1408, 1286, 1244, 1191, 1103, 1100, 932, 898, 868, 809, 716, 662.

Ethynylferrocene was then synthesized according to the literature procedure.[33] Briefly, 1,1-dichloro-2-ferrocenylethene (147 mg, 0.52 mmol) was dissolved in THF (1 mL, anhydrous). The solution was cooled to 0 °C and stirred under dry nitrogen during the dropwise addition of *n*-BuLi (2.24 M in hexanes, 0.43 mL, 1.04 mmol). The reaction was then removed from the ice bath and allowed to stir for 10 min, and was cooled again to 0 °C prior to quenching with Nanopure water (1 mL). The solution was extracted with ether, dried with $MgSO_4$, and the solvent removed under reduced pressure. Purification of the crude product by flash column chromatography was performed using a short column of neutral alumina (9:1 hexanes/dichloromethane) (99.6 mg, 91% yield). mp 52−53 °C (lit. 52−53 °C). ^{1}H NMR (600 MHz, $CDCl_3$) δ 4.48 (t, J = 1.8 Hz, 2H), 4.24 (s, 5H), 4.21 (t, J = 1.8 Hz, 2H), 2.74 (s, 1H). ^{13}C NMR (150 MHz, $CDCl_3$) δ 82.8, 73.8, 71.9, 70.2, 68.9, 64.0. IR (cm^{-1}) 3293, 3095, 2108, 1774, 1647, 1411, 1226, 1106, 1024, 1001, 916, 821, 645, 531.

Alkyne-Stabilized Ruthenium Nanoparticles. The synthetic procedure was outlined in Scheme 1. In a typical reaction, to a two-neck round-bottom flask under dry nitrogen protection was added 1-octyne (0.14 mL, 0.94 mmol) and THF (5 mL, anhydrous). The solution was cooled to −78 °C (acetone/dry ice bath) and stirred prior to the dropwise addition of 2.24 M *n*-BuLi in hexanes (0.42 mL, 0.96 mmol). The reaction was allowed to stir for 1 h to prepare 1-octynyllithium. In a separate flask, ruthenium chloride predried under a vacuum oven and THF (30 mL, anhydrous) was stirred and cooled to −78 °C. The ruthenium salt solution was added to the cooled 1-octynyllithium solution via cannula, and the resulting mixture was allowed to warm to room temperature over a period of 1 h. A 1.0 M solution of lithium triethylborohydride in hexanes (5.0 mL, 5.0 mmol) was added dropwise to the reaction mixture, and the resulting solution exhibited an immediate color change from dark red to dark brown, signifying the formation of Ru nanoparticles. The resulting solution was allowed to stir at room temperature over 3 h. The reaction was cooled with an ice−water bath and quenched with Nanopure water. Solvents were then removed under reduced pressure with a rotary evaporator. The resulting sample was washed several times with copious amounts of ethanol to remove any excess of ligands and other impurities, affording purified nanoparticles (denoted as Ru−OC). The particles were found to be readily soluble in typical apolar solvents such as toluene, THF, chloroform, and dichloromethane, and not soluble in polar solvents such as alcohols, acetone, and acetonitrile.

SCHEME 2

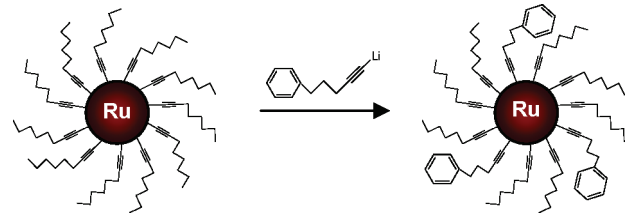

To prepare ferrocene-functionalized ruthenium nanoparticles, the same procedure was used except that a mixture of 1-octyne and ethynylferrocene (molar ratio 7:3) was used as the protecting ligands. The resulting particles were referred to as Ru−OC−Fc. The concentration of the ferrocene functional group on the nanoparticle surface was quantitatively evaluated by ^{1}H NMR measurement by collecting the organic components after dissolution of the Ru cores by dilute KCN. From the ratio of the integrated peak areas of the protons from the ferrocenyl and methyl groups, the surface concentration of the ferrocene moieties on Ru nanoparticles was estimated to be ca. 13%.

Ligand Exchange Reactions. The ligand exchange reaction of the Ru−OC nanoparticles obtained above was exemplified with the acetylide of 5-phenyl-1-pentyne (Scheme 2). Briefly, the cooled lithium−phenylpentyne anion solution in toluene was first prepared by using the same synthetic procedure of the lithium−octyne anion as detailed above. In a separate flask, the Ru−OC nanoparticles in toluene were cooled to −78 °C and then added to the cooled lithium−phenylpentyne anion solution via cannula. The resulting mixture was allowed to warm to room temperature over a period of 1 h and stirred about 3 h. The particles were then dried under reduced pressure and washed by excessive ethanol to remove excessive ligands. The resulting particles were referred to as Ru−PP.

Spectroscopies. Proton and carbon nuclear magnetic resonance (^{1}H and ^{13}C NMR) spectroscopic measurements were carried out by using concentrated solutions of nanoparticles in $CDCl_3$ or CD_2Cl_2 with a Varian Unity 500 MHz NMR spectrometer. UV−vis spectroscopic studies were performed

with an ATI Unicam UV4 spectrometer using a 1 cm quartz cuvette with a resolution of 2 nm. Photoluminescence characteristics were examined with a PTI fluorospectrometer. NIR spectra were acquired with an Ocean Optics NIR-512 spectrometer. FTIR measurements were carried out with a Perkin-Elmer FTIR spectrometer (Spectrum One, spectral resolution 4 cm^{-1}) where the samples were prepared by casting the particle solutions onto a NaCl disk. Thermogravimetric analysis (TGA) was performed in a nitrogen atmosphere with a Perkin-Elmer Pyris 1 TGA thermal analyzer at a heating rate of 10 °C/min.

Transmission Electron Microscopy (TEM). The particle core diameter and lattice fringes were determined with a JEOL-F 200 KV field-emission analytical transmission electron microscope in the Molecular Foundry and the National Center for Electron Microscopy at Lawrence Berkeley National Laboratory. The samples were prepared by casting a drop of the particle solution (~1 mg/mL) in dichloromethane (DCM) onto a 200-mesh holey carbon-coated copper grid.

Electrochemistry. Voltammetric measurements were carried out with a CHI 440 electrochemical workstation. A polycrystalline gold disk electrode (sealed in a glass tubing) was used as the working electrode. A Ag/AgCl wire and a Pt coil were used as the (quasi)reference and counter electrodes, respectively. The gold electrode was first polished with alumina slurries of 0.05 μm and then cleansed by sonication in 0.1 M HNO_3, H_2SO_4, and Nanopure water successively. Prior to data collection, the electrolyte solution was deaerated by bubbling ultra-high-purity N_2 for at least 20 min and blanketed with a nitrogen atmosphere during the entire experimental procedure. Note that the potentials were all calibrated against the formal potential of ferrocene monomers (Fc^+/Fc) in the same solvent.

Results and Discussion

Ru−OC Nanoparticles. In this study, ruthenium nanoparticles were prepared with a protecting monolayer consisting of alkynyl fragments (Scheme 1). It should be noted that alkynes (and alkenes as well) have been used rather extensively as coordinating ligands in the preparation of varied transition metal complexes.[34–37] In comparison with alkenes, alkynes are generally more electropositive and therefore tend to bind more tightly to transition metal centers. Therefore, it is envisioned that the chemical stability of the nanoparticles may be further enhanced with alkynyl fragments as the protecting ligands, leading to ready manipulation of the nanoparticle material properties. Ruthenium nanoparticles passivated by 1-octynyl fragments were used as the illustrating example. As depicted in Scheme 1, 1-octyne was first converted to 1-octynyllithium (OC−Li) by deprotonation reactions with *n*-butyllithium. OC−Li was then used as stabilizing ligands for the passivation of ruthenium metal cores that were formed by the reduction of $RuCl_3$ by superhydride.

The formation of ruthenium nanoparticles was first verified by TEM measurements. Figure 1 depicts a representative TEM micrograph of the Ru−OC nanoparticles prepared above. It can be seen that the Ru nanoparticles were all well dispersed without apparent aggregation, suggesting effective passivation of the alkyne ligands on the Ru particle surfaces. In addition, the majority of the Ru−OC nanoparticles may be found within the narrow range of 2−3 nm in diameter, as depicted in the core-size histogram (figure inset). In fact, statistical analysis based on the measurements of more than 700 particles shows the average particle core diameter is 2.55 ± 0.15 nm. Furthermore, lattice fringes of 0.230 nm can be clearly resolved, which are attributed to the Ru(100) crystalline planes. This further confirms the formation of nanosized Ru metal cores.

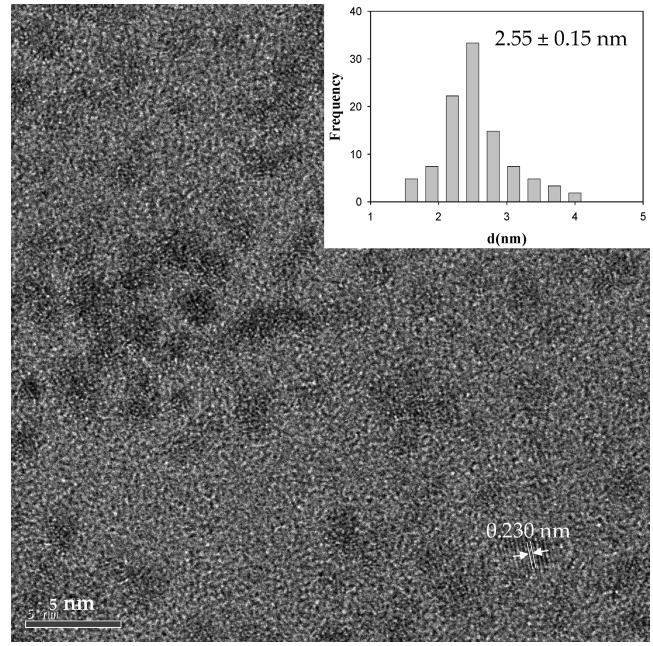

Figure 1. Representative TEM micrograph of Ru−OC nanoparticles. Scale bar 5 nm. Lattice fringes of 0.230 nm were identified in the figure. The inset shows the core size histogram.

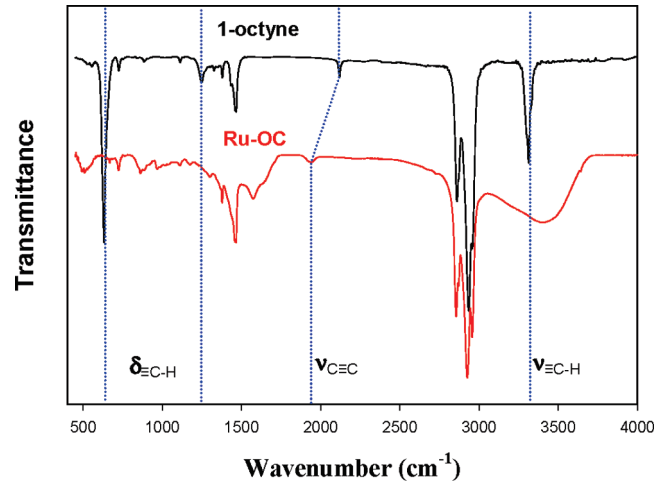

Figure 2. FTIR spectra of 1-octyne (black curve) and Ru−OC nanoparticles (red curve).

The structure of the particle-bound octynyl fragments was then examined by FTIR measurements. Figure 2 depicts the FTIR spectra of monomeric 1-octyne and Ru−OC. For monomeric 1-octyne (black curve), four characteristic bands can be identified at 3313 cm^{-1} (alkynyl ≡C−H stretch), 2119 cm^{-1} (C≡C stretch), 1255 cm^{-1} (≡C−H bend overtone), and 631 cm^{-1} (≡C−H bend fundamental).[38] In sharp contrast, upon deprotonation and binding onto the Ru nanoparticle surface (red curve), the ≡C−H stretching and bending bands disappear (the broad band centered around 3500 cm^{-1} most likely arose from residual water) and the C≡C stretch red-shifts to 1936 cm^{-1}. It should be noted that the C≡C stretch of monomeric alkynes is typically observed as a weak band within the range 2100−2260 cm^{-1}.[38] However, when alkynes are coordinated to a transition metal center, generally the C≡C bonding order decreases, leading to an apparent red-shift of the stretching vibration to the range 1700−2000 cm^{-1}.[39] The experimental observation presented in Figure 2 is consistent with these earlier studies (note also that the normal aliphatic C−H vibrational stretches

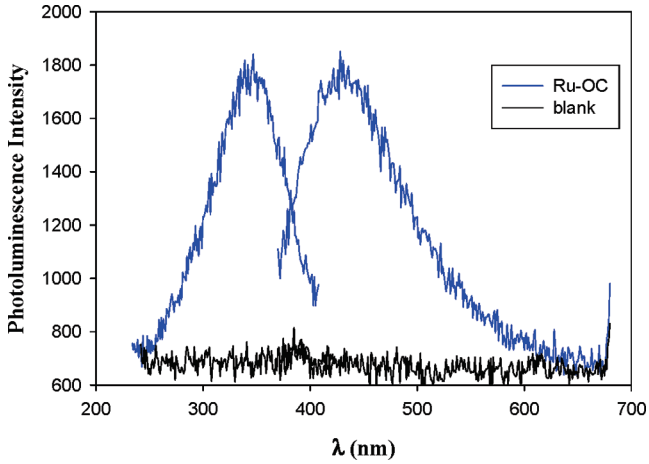

Figure 3. Excitation and emission spectra of Ru−OC nanoparticles (blue curves) at a concentration of 0.1 mg/mL in DCM. The corresponding profiles measured with the blank solvent (black curves) were also included.

within the range 2850−2950 cm^{-1} remained virtually unchanged between the monomeric 1-octyne and Ru−OC nanoparticles), suggesting that the octynyl fragments were indeed bound onto the Ru metal surface.

The surface coverage of the 1-octynyl fragments was then evaluated by TGA measurements (Figure S1 in the Supporting Information). Ligand desorption was found to commence at ca. 150 °C and continue until 300 °C, with total weight loss of about 18.2%. For nanoparticles with an average core diameter of 2.55 nm (Figure 1), this corresponds to approximately 133 1-octynyl ligands per particle, or an average footprint area of 0.15 nm^2 per ligand on the nanoparticle surface. Note that this is somewhat smaller than that observed, for instance, for alkanethiolates adsorbed on gold surfaces (0.214 nm^2),[40] which is not unreasonable considering the smaller cross-sectional area of the sp carbons.[41]

Interestingly, the Ru−OC nanoparticles exhibited unique photoluminescence properties, whereas UV−visible absorption measurements depicted only a featureless exponential decay profile (Figure S2, Supporting Information), as anticipated for nanosized Ru particles.[27] Figure 3 shows the excitation and emission spectra (blue curves) of the Ru−OC nanoparticles at a concentration of 0.1 mg/mL in DCM, along with those of the blank solvent (black curves). Very well-defined excitation and emission peaks can be seen at 347 and 428 nm, respectively. This is in sharp contrast with previous studies of Ru nanoparticles passivated by either carbene or aryl fragments where no apparent photoluminescence was observed.[27,29,30,32] It should be noted that dimers, trimers, and polymers of acetylene typically exhibit a fluorescence emission peak at around 408 nm,[42] which is very close to that observed above for the Ru−OC nanoparticles (428 nm). Since the Ru cores are large enough (Figure 1) to act as a conducting medium, the acetylene moieties bound onto the Ru particle surface may be considered to behave equivalently to −C≡C−C≡C−. That is, the photoluminescence observed with the Ru−OC nanoparticles strongly suggests that intraparticle charge delocalization took place as a result of the strong Ru−C≡ interfacial bonding interactions.

One may argue that the photoluminescence might also be attributable to oligomeric/polymeric derivatives of 1-octyne formed during the nanoparticle synthesis. However, this hypothesis is highly unlikely. First of all, the Ru−OC nanoparticles had been subjected to extensive rinsing to remove excessive ligands and organic byproducts before experimental characterizations were carried out, and the purity of the nanoparticles was verified by careful NMR measurements. Figure 4 shows the ^{1}H NMR spectra of (A) monomeric 1-octyne molecules and (B) Ru−OC nanoparticles. First, it can be seen that all protons in 1-octyne may be accounted for in curve A: (a_1) 0.9 ppm, CH_3; (b_1) 1.1−1.6 ppm, $(CH_2)_4CH_3$; (c_1) 2.2 ppm, $CH_2C{\equiv}CH$; and (d_1) 1.9 ppm, $C{\equiv}CH$. In contrast, for Ru−OC nanoparticles, only peaks a_1 and b_1 remain and both are drastically broadened as compared to their counterparts in curve A. The observation is consistent with the deprotonation of 1-octyne and the subsequent binding of the 1-octynyl fragment onto Ru nanoparticle surfaces, as it is a well-known phenomenon that, when organic capping ligands are bound onto nanoparticle surfaces, their corresponding NMR features become broadened and the broadening is more significant for protons that reside closer to the metal core surface.[22,27,43] Thus, typically only the peripheral protons (e.g., a_1 and b_1 protons) may be resolved, whereas the inner ones are broadened into baseline (e.g., c_1 protons). The fact that only a_1 and b_1 protons of Ru−OC nanoparticles were resolved in NMR measurements also suggests that the nanoparticles were indeed free of any excessive ligands or organic byproducts. Consistent behaviors were observed in ^{13}C NMR measurements (Figure S3, Supporting Information).

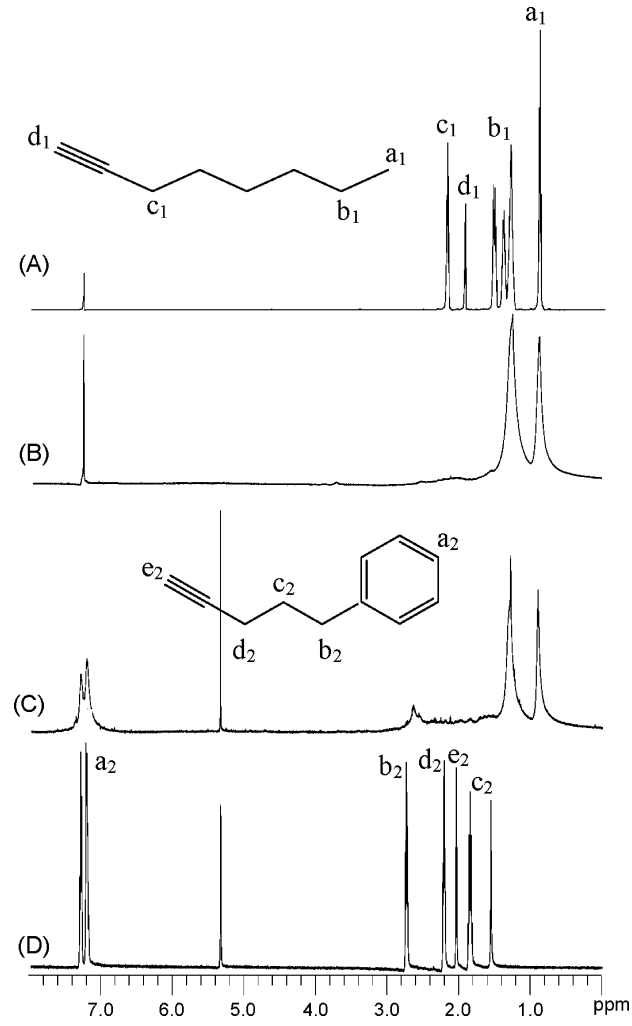

Figure 4. ^{1}H NMR spectra of Ru nanoparticles before (Ru−OC) and after ligand exchange reaction (Ru−PP): (A) monomeric 1-octyne ligands; (B) Ru−OC particles; (C) Ru−PP particles; (D) monomeric 5-phenyl-1-pentyne. The solvents were either $CDCl_3$ (A and B) or CD_2Cl_2 (C and D). The ligand molecular structures are labeled in the figure.

Additionally, a control experiment was carried out where the identical procedure in Scheme 1 was followed except for the addition of $RuCl_3$, and the resulting solution exhibited no detectable photoluminescence under the same experimental conditions as those in Figure 3. This indicates that Ru−OC nanoparticles alone are responsible for the photoluminescence characteristics depicted in Figure 3.

In short, these experimental observations suggest that the nanoparticle photoluminescence most likely arose from the strong Ru−C≡ interfacial bonding interactions that led to the formation of extended conjugation between particle-bound functional moieties, akin to that observed with Ru nanoparticles passivated by Ru=carbene π bonds.[4,28,31]

Ligand Exchange Reactions. Interestingly, the Ru−OC nanoparticles could be further functionalized by ligand exchange reactions with acetylene-terminated derivatives, as outlined in Scheme 2. In the present study, 5-phenyl-1-pentyne was chosen as the illustrating example. Experimentally, 5-phenyl-1-pentyne was first converted into 5-phenyl-1-pentynyllithium by reacting with *n*-BuLi, which was then mixed with Ru−OC nanoparticles to initiate ligand exchange. The resulting particles were then purified and collected for experimental characterizations. Figure 4C shows the ^{1}H NMR spectrum of Ru−OC nanoparticles that had undergone exchange reactions with 5-phenyl-1-pentyne for 6 h. In comparison with the NMR spectrum of monomeric 5-phenyl-1-pentyne in curve D, the broad peaks at $\delta = 7.2-7.3$ ppm may be assigned to the phenyl protons (a_2) and that at $\delta = 2.6-2.7$ ppm to the methylene protons (b_2) next to the terminal phenyl group (−CH_2−Ph). Note that the disappearance of the c_2, d_2, and e_2 protons (*H*C≡C−CH_2−CH_2−) is again consistent with the deprotonation of the terminal C≡C−H group and the broadening of the NMR features into the baseline for protons close to the Ru cores. Similar behaviors were observed in ^{13}C NMR measurements (Figure S3, Supporting Information). These experimental results indicate that the 5-phenyl-1-pentynyl ligands were successfully incorporated onto the Ru−OC particle surface. The appearance of the methyl protons at $\delta = 0.9$ ppm (a_1) signifies that not all the original 1-octynyl ligands were replaced by the 5-phenyl-1-pentynyl fragments. From the ratio of the integrated peak areas of the methyl and phenyl protons, the extent of exchange may be estimated to be 40.2%; namely, 40.2% of the original octynyl ligands on the Ru nanoparticle surface were replaced with the 5-phenyl-1-pentynyl counterparts.

Note that the nanoparticle core diameter remained practically unchanged after ligand exchange reactions, as determined by TEM measurements. So did the photoluminescence characteristics, consistent with the fact that the photoemission was mainly attributable to the interfacial −C≡C− groups (vide ante).

Ru−OC−Fc Nanoparticles. The impacts of the Ru−C≡ interfacial bonding interactions on intraparticle charge delocalization were further examined by using ruthenium nanoparticles functionalized with a mixed monolayer of 1-octyne and ethynylferrocene (Ru−OC−Fc). Figure 5 shows the representative differential pulse voltammograms (DPVs) of the Ru−OC and Ru−OC−Fc nanoparticles, respectively, in DCM with 0.10 M tetrabutylammonium perchlorate (TBAP) as the supporting electrolyte. It can be seen that their voltammetric characteristics are drastically different. Whereas Ru−OC nanoparticles (red curve) exhibited a largely featureless profile that did not differ much from that of the blank electrolyte (black curve), two pairs of voltammetric peaks are rather well-defined with the Ru−OC−Fc nanoparticles (green curve) with formal potentials ($E^{\circ\prime}$) of +0.078 and +0.343 V (vs Fc^+/Fc). These are ascribed to the redox reactions of the ferrocene moieties bound on the

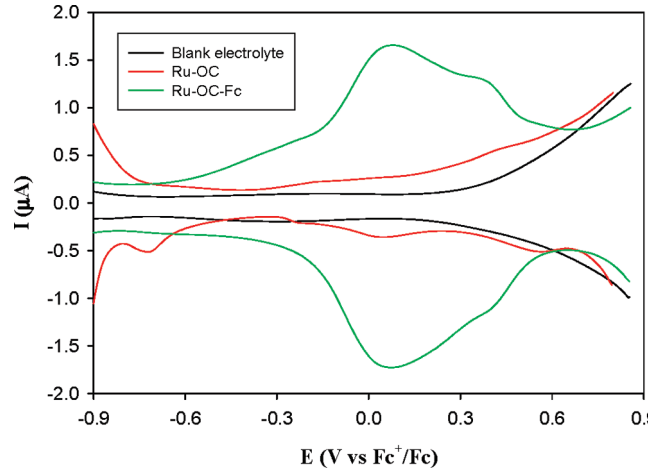

Figure 5. Differential pulse voltammograms (DPVs) of Ru−OC (red curve) and Ru−OC−Fc (green curve) nanoparticles in dichloromethane (DCM) containing 0.1 M tetrabutylammonium perchlorate (TBAP). The particle concentrations were both 8 mg/mL. The DPV profiles of the blank electrolyte (black curve) were also included in the figure. Au disk electrode area 0.8 mm^2. In the DPV measurements, the dc ramp was 4 mV/s, the pulse amplitude was 50 mV, and the pulse width was 200 ms.

nanoparticle surface, $Fc^+ + e \leftrightarrow Fc$. The appearance of two pairs of voltammetric peaks, instead of one that is anticipated with monomeric ferrocene, strongly suggests that interfacial intervalence transfer occurs between the ferrocene groups through the metallic ruthenium cores. Additionally, the potential spacing ($\Delta E^{\circ\prime}$) of 265 mV is highly comparable to those of biferrocene derivatives with a conjugated chemical linker,[31,44−46] suggesting class II behaviors as defined by Robin and Day.[47] Furthermore, the somewhat larger $\Delta E^{\circ\prime}$, as compared to that observed with Ru=carbene π bonds,[4,31] indicates that the intraparticle charge delocalization was better facilitated by the Ru−C≡ interfacial bonding interactions. Note that strong electronic couplings have been observed in a series of organometallic complexes where two terminal ferrocenyl moieties were connected by a bis-ethynyl/butadiynyl diruthenium bridge, i.e., Fc−$(C\equiv C)_n$−Ru_2−$(C\equiv C)_m$−Fc with *n* and *m* equal to 1 or 2, and at $n = m = 1$, $\Delta E^{\circ\prime}$ was found to be around 300 mV.[48]

The intervalence charge-transfer characteristics of Ru−OC−Fc nanoparticles were further confirmed in near-IR spectroscopic measurements by using nitrosonium tetrafluoroborate ($NOBF_4$) as the oxidizing reagent. Figure 6 shows the NIR absorption spectra of Ru−OC−Fc nanoparticles in CH_2Cl_2 with the addition of varied amounts of freshly prepared 1 mM $NOBF_4$ in CH_2Cl_2. It can be seen that, with the addition of $NOBF_4$, a new absorption band centered around 1687 nm starts to appear (the wavy features may be due to instrumental artifacts, but the exact origin is not clear at this point), and the peak absorbance exhibits a volcano-shaped variation with the amount of oxidant added (figure inset). Such an NIR absorption feature is very analogous to that observed with Ru nanoparticles functionalized with ferrocene moieties through Ru−carbene π bonds,[4] again strongly supporting the notion that intraparticle intervalence charge transfer indeed occurred between the ferrocene groups at mixed valence. In other words, electronic communication between nanoparticle-bound ferrocene moieties may be effected by highly delocalized interfacial bonding interactions such as Ru−C≡ and Ru=C bonds. For comparison, very similar NIR responses were also observed with monocations of Fc−C≡C−Fc[49] and Fc−C≡C−Ru_2−C≡C−Fc,[48] which exhibited a well-defined NIR absorption band at 1620 nm (in CH_2Cl_2) and 1667 nm (in THF), respectively.

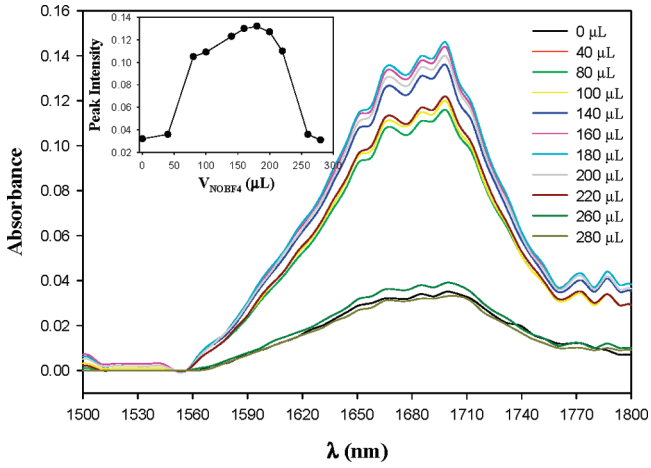

Figure 6. Near-IR spectra of Ru−OC−Fc nanoparticles with the addition of varied amounts of 1 mM $NOBF_4$ (shown as figure legends). The inset shows the variation of the peak absorbance at 1687 nm with the amount of $NOBF_4$ added. The particle concentration was 0.1 mg/mL in DCM.

Conclusion

Stable ruthenium nanoparticles were prepared by using 1-octynyl fragments as the protecting ligands through the formation of Ru−C≡ interfacial bonding interactions. Lattice fringes of the nanoparticle cores revealed in TEM measurements were consistent with metallic ruthenium. The binding of the octynyl fragments onto the nanoparticle surface was confirmed in FTIR, TGA, and NMR spectroscopic measurements. Notably, the C≡C vibrational stretch was found to red-shift as compared to that of monomeric 1-octyne because of the formation of Ru−C≡ bonds; in ^1H and ^{13}C NMR measurements, only the terminal methyl and methylene groups were resolved, consistent with the broadening characteristics of nanoparticle-bound ligands; and TGA measurements suggested that the nanoparticle cores were protected by a compact layer of the octynyl fragments. Additionally, the resulting particles exhibited well-defined photoluminescence characteristics that were analogous to diacetylene compounds, suggesting that the Ru−C≡ bonds might serve as effective pathways for intraparticle extended conjugation. This is further manifested in the electrochemical and NIR spectroscopic studies of ruthenium nanoparticles that were functionalized with a mixed monolayer of 1-octyne and ethynylferrocene. Both measurements showed that effective intervalence transfer indeed occurred between the particle-bound ferrocenyl moieties at mixed valence and the behaviors were consistent with those of conventional organometallic complexes as well as nanoparticles functionalized with ferrocenyl moieties by Ru−carbene π bonds, further signifying the fundamental significance of metal−ligand interfacial bonding interactions on the nanoparticle material properties.

As the nanoparticles can undergo ligand exchange reactions with alkynyl lithium, it is envisioned that the optoelectronic properties of the nanoparticles may be further manipulated through controlled chemical functionalization. Research along this direction is underway.

Note Added after ASAP Publication. Due to a production error, this manuscript was inadvertently omitted from the special issue "Protected Metallic Clusters, Quantum Wells and Metal-Nanocrystal Molecules Symposium", published as the September 30, 2010, issue of *J. Phys. Chem. C* (Vol. 114, issue 38; URL: http://pubs.acs.org/toc/jpccck/114/38). ACS Publications sincerely apologizes for this oversight.

Acknowledgment. This work was supported by the National Science Foundation through grants CHE-0708170 and CHE-0832605. D.G. is an NSF ACC-F postdoctoral fellow. TEM micrographs were acquired by using the TEM facility at the Molecular Foundry, Lawrence Berkeley National Laboratory, which is supported by the US Department of Energy.

Supporting Information Available: TGA, UV−vis absorption, and ^{13}C NMR spectra of Ru−OC and Ru−PP nanoparticles. This material is available free of charge via the Internet at http://pubs.acs.org.

References and Notes

(1) Schmid, G. *Chem. Rev.* **1992**, *92*, 1709–1727.
(2) Murray, R. W. *Chem. Rev.* **2008**, *108*, 2688–2720.
(3) Daniel, M. C.; Astruc, D. *Chem. Rev.* **2004**, *104*, 293–346.
(4) Chen, W.; Chen, S. W.; Ding, F. Z.; Wang, H. B.; Brown, L. E.; Konopelski, J. P. *J. Am. Chem. Soc.* **2008**, *130*, 12156–12162.
(5) Andres, R. P.; Bein, T.; Dorogi, M.; Feng, S.; Henderson, J. I.; Kubiak, C. P.; Mahoney, W.; Osifchin, R. G.; Reifenberger, R. *Science* **1996**, *272*, 1323–1325.
(6) Chen, S. W.; Ingram, R. S.; Hostetler, M. J.; Pietron, J. J.; Murray, R. W.; Schaaff, T. G.; Khoury, J. T.; Alvarez, M. M.; Whetten, R. L. *Science* **1998**, *280*, 2098–2101.
(7) Berven, C. A.; Clarke, L.; Mooster, J. L.; Wybourne, M. N.; Hutchison, J. E. *Adv. Mater.* **2001**, *13*, 109–113.
(8) Chen, W.; Chen, S. W. *Angew. Chem., Int. Ed.* **2009**, *48*, 4386–4389.
(9) Mohr, C.; Hofmeister, H.; Radnik, J.; Claus, P. *J. Am. Chem. Soc.* **2003**, *125*, 1905–1911.
(10) Turner, M.; Golovko, V. B.; Vaughan, O. P. H.; Abdulkin, P.; Berenguer-Murcia, A.; Tikhov, M. S.; Johnson, B. F. G.; Lambert, R. M. *Nature* **2008**, *454*, 981–U31.
(11) Lewis, L. N. *Chem. Rev.* **1993**, *93*, 2693–2730.
(12) Tsunoyama, H.; Sakurai, H.; Negishi, Y.; Tsukuda, T. *J. Am. Chem. Soc.* **2005**, *127*, 9374–9375.
(13) Mirkin, C. A.; Letsinger, R. L.; Mucic, R. C.; Storhoff, J. J. *Nature* **1996**, *382*, 607–609.
(14) Emery, S. R.; Haskins, W. E.; Nie, S. M. *J. Am. Chem. Soc.* **1998**, *120*, 8009–8010.
(15) Zayats, M.; Kharitonov, A. B.; Pogorelova, S. P.; Lioubashevski, O.; Katz, E.; Willner, I. *J. Am. Chem. Soc.* **2003**, *125*, 16006–16014.
(16) Schwerdtfeger, P. *Angew. Chem., Int. Ed.* **2003**, *42*, 1892–1895.
(17) Whetten, R. L.; Shafigullin, M. N.; Khoury, J. T.; Schaaff, T. G.; Vezmar, I.; Alvarez, M. M.; Wilkinson, A. *Acc. Chem. Res.* **1999**, *32*, 397–406.
(18) Huang, T.; Murray, R. W. *J. Phys. Chem. B* **2001**, *105*, 12498–12502.
(19) Chen, W.; Zuckerman, N. B.; Konopelski, J. P.; Chen, S. W. *Anal. Chem.* **2010**, *82*, 461–465.
(20) Sun, S. H.; Murray, C. B.; Weller, D.; Folks, L.; Moser, A. *Science* **2000**, *287*, 1989–1992.
(21) Sun, T.; Seff, K. *Chem. Rev.* **1994**, *94*, 857–870.
(22) Hostetler, M. J.; Wingate, J. E.; Zhong, C. J.; Harris, J. E.; Vachet, R. W.; Clark, M. R.; Londono, J. D.; Green, S. J.; Stokes, J. J.; Wignall, G. D.; Glish, G. L.; Porter, M. D.; Evans, N. D.; Murray, R. W. *Langmuir* **1998**, *14*, 17–30.
(23) Chen, S. W.; Murray, R. W.; Feldberg, S. W. *J. Phys. Chem. B* **1998**, *102*, 9898–9907.
(24) Montalti, M.; Zaccheroni, N.; Prodi, L.; O'Reilly, N.; James, S. L. *J. Am. Chem. Soc.* **2007**, *129*, 2418–+.
(25) Templeton, A. C.; Cliffel, D. E.; Murray, R. W. *J. Am. Chem. Soc.* **1999**, *121*, 7081–7089.
(26) Templeton, A. C.; Wuelfing, M. P.; Murray, R. W. *Acc. Chem. Res.* **2000**, *33*, 27–36.
(27) Chen, W.; Davies, J. R.; Ghosh, D.; Tong, M. C.; Konopelski, J. P.; Chen, S. W. *Chem. Mater.* **2006**, *18*, 5253–5259.
(28) Chen, W.; Zuckerman, N. B.; Lewis, J. W.; Konopelski, J. P.; Chen, S. W. *J. Phys. Chem. C* **2009**, *113*, 16988–16995.
(29) Ghosh, D.; Chen, S. W. *J. Mater. Chem.* **2008**, *18*, 755–762.
(30) Ghosh, D.; Chen, S. W. *Chem. Phys. Lett.* **2008**, *465*, 115–119.
(31) Chen, W.; Brown, L. E.; Konopelski, J. P.; Chen, S. W. *Chem. Phys. Lett.* **2009**, *471*, 283–285.
(32) Ghosh, D.; Pradhan, S.; Chen, W.; Chen, S. W. *Chem. Mater.* **2008**, *20*, 1248–1250.
(33) Luo, S. J.; Liu, Y. H.; Liu, C. M.; Liang, Y. M.; Ma, Y. X. *Synth. Commun.* **2000**, *30*, 1569–1572.
(34) Furstner, A.; Davies, P. W. *Angew. Chem., Int. Ed.* **2007**, *46*, 3410–3449.

(35) Yamamoto, Y. *J. Org. Chem.* **2007**, *72*, 7817–7831.
(36) Rosenthal, U.; Oehme, G.; Burlakov, V. V.; Petrovskii, P. V.; Shur, V. B.; Volpin, M. E. *J. Organomet. Chem.* **1990**, *391*, 119–122.
(37) Casey, C. P.; Lee, T. Y.; Tunge, J. A.; Carpenetti, D. W. *J. Am. Chem. Soc.* **2001**, *123*, 10762–10763.
(38) Silverstein, R. M.; Bassler, G. C.; Morrill, T. C. *Spectrometric identification of organic compounds*; 5th ed.; Wiley: New York, 1991.
(39) Back, S.; Gossage, R. A.; Rheinwald, G.; del Rio, I.; Lang, H.; van Koten, G. *J. Organomet. Chem.* **1999**, *582*, 126–138.
(40) Sellers, H.; Ulman, A.; Shnidman, Y.; Eilers, J. E. *J. Am. Chem. Soc.* **1993**, *115*, 9389–9401.
(41) Mikhailov, B. M. *Russ. Chem. Bull.* **1960**, *9*, 1284–1290.
(42) Warta, R.; Sixl, H. *J. Chem. Phys.* **1988**, *88*, 95–99.
(43) Terrill, R. H.; Postlethwaite, T. A.; Chen, C. H.; Poon, C. D.; Terzis, A.; Chen, A. D.; Hutchison, J. E.; Clark, M. R.; Wignall, G.; Londono, J. D.; Superfine, R.; Falvo, M.; Johnson, C. S.; Samulski, E. T.; Murray, R. W. *J. Am. Chem. Soc.* **1995**, *117*, 12537–12548.
(44) Brown, G. M.; Meyer, T. J.; Cowan, D. O.; Levanda, C.; Kaufman, F.; Roling, P. V.; Rausch, M. D. *Inorg. Chem.* **1975**, *14*, 506–511.
(45) Levanda, C.; Cowan, D. O.; Bechgaard, K. *J. Am. Chem. Soc.* **1975**, *97*, 1980–1981.
(46) Kadish, K. M.; Xu, Q. Y.; Barbe, J. M. *Inorg. Chem.* **1987**, *26*, 2565–2566.
(47) Robin, M. B.; Day, P. *Adv. Inorg. Chem. Radiochem.* **1967**, *10*, 247–422.
(48) Xu, G. L.; Crutchley, R. J.; DeRosa, M. C.; Pan, Q. J.; Zhang, H. X.; Wang, X. P.; Ren, T. *J. Am. Chem. Soc.* **2005**, *127*, 13354–13363.
(49) Powers, M. J.; Meyer, T. J. *J. Am. Chem. Soc.* **1978**, *100*, 4393–4398.

JP101053C